Luminescence and Single-Molecule Magnet Properties in Ideal Symmetry Compounds: Example of a Near-Planar Tricoordinate Ytterbium(III) Amide

Nimisha Jain, Félix Houard, Rémi Marchal, Marie Cordier, Boris Le Guennic, Yan Suffren, Yann Sarazin, Kevin Bernot

ChemistryEurope
Excellence in Chemistry Research Worldwide

Research Article
doi.org/10.1002/ceur.202400062

www.journal.chemistry-europe.org

Luminescence and Single-Molecule Magnet Properties in Ideal Symmetry Compounds: Example of a Near-Planar Tricoordinate Ytterbium(III) Amide

Nimisha Jain,[a] Félix Houard,[a] Rémi Marchal,[a] Marie Cordier,[a] Boris Le Guennic,[a] Yan Suffren,[a] Yann Sarazin,*[a] and Kevin Bernot*[a]

This work is dedicated to the memory of Pr. Miguel Julve, passionate teacher, researcher and mentor

We are reporting on the use of a low-coordinate Yb^{III} amide with near-ideal planar trigonal $[Yb\{N(SiMe_3)_2\}_3]$ (**1**) and on a bipyramidal trigonal derivative $[Yb\{N(SiMe_2H)_2\}_3\cdot(thf)_2]$ (**2**) that constitute quintessential cases to investigate luminescent and magnetic properties otherwise usually blurred on less symmetrical compounds. These compounds represent the first experimental objects that allow for the confirmation of the recent conjecture about best-performing SMM built on the archetypal prolate lanthanide ion. We have performed a combined theoretical, luminescent, and magnetic study on these molecules. For **1**, a spectacular split of the $^2F_{7/2}$ ground state of 1312 cm^{-1} is measured by low-temperature near-infrared luminescence as well as the calculated pure wavefunction composition of the low-lying Kramers doublets, making this complex a textbook example of a prolate SMM. These results are corroborated by comparison with **2**, that exhibits as expected a 50% decrease of the ground state splitting compared to **1**. Yet, we show that these remarkable features are insufficient to promote SMM behavior, and Orbach relaxation is unlikely to occur even on such an ideal low-coordinate SMM without control of spin-phonon coupling.

Introduction

Lanthanide-based single-molecule magnets (4*f*-SMMs)[1] are a promising class of magnetic molecules, because of their unique magnetic properties and potential applications in high-density magnetic data storage, quantum computing, and spintronics, among other areas. These molecules exhibit slow magnetic relaxation and magnetic memory of molecular origin and are built around lanthanide ions, which are characterized by their very large magnetic moments and magnetic anisotropy, coordinated by organic ligands.

Proper optimization of the coordination geometry and the resulting electrostatic environment around a given *4f* ion allows for the harnessing of its magnetic anisotropy by stabilizing its most anisotropic M_J states. 4*f* ions can be categorized, depending of the preferential shape of their free-ion electron density, as oblate (Ce^{III}, Pr^{III}, Nd^{III}, Tb^{III}, Dy^{III}, Ho^{III}) or prolate (Sm^{III}, Er^{III}, Tm^{III}, Yb^{III}).[2] As magnetic bistability is favored with Kramer ions (half-integer *J*), Dy^{III} ($J=15/2$) and Yb^{III} ($J=7/2$) are the most popular ions to build respectively oblate-based or prolate-based SMMs. Other ions and oxidation states are far less studied[3] with the exception of Tb^{III} in highly symmetric environments such as Tb-phthalocyanine derivatives,[4] as well as divalent Tm^{II}[5] and Eu^{II}.[6]

The direct consequence of these magnetic anisotropy considerations is that best SMM performances are achieved when oblate ions are involved in an axial coordination geometry, whereas prolate ions require an equatorial environment.[7] These environments are best optimized in low-coordinate 4*f* molecules[8] with, for example, a Dy^{III} (*i.e.* oblate ion) bis-coordinated in an axial way[9] or a Yb^{III} (*i.e.* prolate ion) tris-coordinated in an equatorial way.[10]

Huge efforts have been paid toward the optimization of the coordination environment of Dy^{III}-SMM toward axiality, resulting in spectacular magnetic hysteresis in the liquid N_2 region.[11] Very recently, a long-theorized,[12] almost perfectly linear two-coordinate Dy^{III}-SMM has finally been obtained.[9a] Unfortunately, the optimal geometry of the molecule is counterbalanced by its low stiffness, which favors under-barrier magnetic relaxation. In comparison with Dy^{III}, few studies have been conducted on the geometric optimization of low-coordinate Yb^{III}-SMM.[13] This mostly results from the fact that low-coordinate equatorial *4f* molecules are particularly tedious to design, owing to the difficulty in guaranteeing steric hindrance out of the coordination plane of the Yb^{III} ion.

The energy level scheme of $4f^n$ ions results from the influence of interelectronic repulsion (producing ^{2S+1}L levels) and spin-orbit coupling ($^{2S+1}L_J$) where *S* and *L* are the spin and orbital total angular momentum quantum numbers respec-

[a] Dr. N. Jain, Dr. F. Houard, R. Marchal, M. Cordier, Dr. B. Le Guennic, Dr. Y. Suffren, Dr. Y. Sarazin, Prof. K. Bernot
Univ Rennes, INSA Rennes, CNRS, ISCR (Institut des Sciences Chimiques de Rennes), UMR 6226, Université de Rennes, Rennes, FRANCE
E-mail: Kevin.Bernot@insa-rennes.fr
yann.sarazin@univ-rennes.fr

Supporting information for this article is available on the WWW under https://doi.org/10.1002/ceur.202400062

Research Article
doi.org/10.1002/ceur.202400062

tively, and J the total angular momentum can take values as $|L-S| \leq J \leq |L+S|$. The ligand field further lifts the degeneracy and each split level is then characterized by an azimuthal projection of J and identified by a M_J number. For odd electronic configurations such as Dy^{III} and Yb^{III}, each M_J level remains doubly degenerate forming a Kramer doublet (KD). These KD can be split only by the application of a magnetic field (Zeeman effect). Accordingly, beyond magnetic properties, the ligand field has, by definition, an impact on the luminescence properties of 4*f*-based molecules[14] made of luminescent ions (all $4f^n$ ions but La^{III}, Gd^{III} and Lu^{III}). Thus, it is relatively easy to characterize the splitting of the M_J levels of 4*f*-SMMs by emission spectroscopy to validate theoretical calculations,[15] and to compare them with the specific parameters extracted from the examination of their magnetic relaxation.[16] This strategy is especially efficient with SMMs, whose magnetic relaxation is governed by several regimes (Orbach, Raman, Quantum Tunneling of the Magnetization (QTM), direct)[17] depending on the temperature region, and where unique and robust sets of fitting parameters are difficult to find. Indeed, Orbach parameters are directly accessible from the M_J level splitting observed by luminescence.[18] This is a useful approach to decouple the quality of splitting from the quality of magnetic relaxation, which can be hence very different.

Yb^{III}-SMMs exhibit rather weak SMM behavior mainly because most of them were simply obtained by the substitution of their parent Dy^{III}-SMMs with no particular optimization of the molecular geometry and electrostatic surroundings. Because Dy^{III} and Yb^{III} have opposite electrostatic environment requisites, the latter behave badly. SMM and their characteristic relaxation time are fitted as $\tau^{-1} = \tau^{-1}_{Direct} + \tau^{-1}_{Raman} + \tau^{-1}_{Orbach} + \tau^{-1}_{QTM} = AT H^m + CT^n + \tau_0^{-1}\exp(-U_{eff}/k_BT) + \tau^{-1}_{QTM}$ (eq.1). Three main features emerge from the available data about Yb^{III}-SMM:[3b] i) all molecules require an external static field to display magnetic relaxation; ii) when identified, Orbach-like relaxation is always observed on a narrow temperature range and followed by Raman-like relaxation at lower temperature; and iii) U_{eff} energy barrier values for magnetic relaxation via Orbach process are rather small, at best $U_{eff} = 54.7$ K (38 cm^{-1}) as observed on [Yb(trensal)].[19] It is worth noting that for this last example, the authors unambiguously show that considering such U_{eff} value is suspicious and incompatible with their spectroscopic observations of M_J splitting.

In 2021, Ruiz and coworkers[10] revealed an inspiring study on model Yb^{III} molecules and showed how M_J splitting evolves with the coordinating geometry, as performed in 2015 on Dy^{III}-SMMs.[20] As expected, the highest splitting was observed for equatorial-like coordination and ideally for a trigonal planar environment made of monodentate anionic ligand. In this case, tris-coordinated Yb^{III} exhibited pure $M_J = 7/2$ as the ground state with very high anisotropy (close to g_z max = 8 μ_B) and total M_J splitting above 1,600 cm^{-1} with ground state and first excited state separated by ca. 1,000 cm^{-1}. It is worth noting that additional coordination of two apical neutral ligands that provide a trigonal bipyramidal environment preserved the high g_z but halved the M_J splitting. However, the authors stated that *"there are no complexes with the same charge distribution that the synthetic targets predicted by our calculations.*

In the present study, we set out to produce such complexes with a tris(amide) $[Yb\{N(SiMe_3)_2\}_3]$ (**1**) as a model of the trigonal planar environment expected to be the more efficient for Yb^{III}-SMM. This complex is the Yb^{III} analogue of the already reported equatorially coordinated Dy^{III} and Er^{III} complexes $[Ln\{N(SiMe_3)_2\}_3]$ theoretically[21] and experimentally.[22] We further report on the solvated tris(amide) $[Yb\{N(SiMe_2H)_2\}_3\cdot(thf)_2]$ (**2**) and tris(siloxide) $[Yb\{OSi(SiMe_3)_3\}_3\cdot(thf)_2]$ (**3**) for comparison as models of the trigonal bipyramidal environment in N_3O_2 and O_5 coordination, respectively.

Results and Discussion

Chemical Design and Crystal Structures

The known[23] tris(amide) $[Yb\{N(SiMe_3)_2\}_3]$ (**1**) was isolated as lemon-yellow single-crystals in 57% yield upon the stoichiometric reaction of $YbCl_3$ and $[LiN(SiMe_3)_2]$ in thf. Its identity was corroborated by SC-XRD analysis, and its purity was confirmed by NMR spectroscopy; the complex is devoid of coordinated solvent. In contrast, the five-coordinate $[Yb\{N(SiMe_2H)_2\}_3\cdot(thf)_2]$ (**2**),[24] obtained through aminolysis of **1** with $HN(SiMe_2H)_2$ in thf, contains two metal-bound thf molecules. It crystallized in 48% yield as colorless prisms suitable for SC-XRD crystallography. The presence of coordinated solvent molecules in **2** is the outcome of the decrease of steric bulk of the amides around the metal ion in comparison with those in **1**. Note that in our hands, the reported salt metathesis procedure[24] between $YbCl_3$ and $[LiN(SiMe_2H)_2]$ did not allow for the crystallization of **2**; instead, we were only able to isolate colorless, block-shaped crystals of the ate complex $[Yb\{N(SiHMe_2)_2\}_4]^-[Li(thf)_4]^+$ (**7**) in 45% yield (*vs* Yb). The ^1H NMR spectrum in thf-d_8 at 298 K of this paramagnetic salt features diagnostic resonances at δ_{1H} 63.9 (Si*H*) and −3.7 (CH_3) ppm, while the ^7Li spectrum exhibits a single, very sharp resonance at δ_{7Li} −0.26 ppm. In our endeavors to obtain soluble, stable compounds amenable to magnetic and luminescent investigations, we also prepared the tris(siloxide) $[Yb\{OSi(SiMe_3)_3\}_3\cdot(thf)_2]$ (**3**), by reaction of **1** with the bulky silanol $(Me_3Si)_3SiOH$ in thf. This known complex[25] was isolated in 58% yield as rod-shaped single crystals upon recrystallization from a concentrated thf solution. For comparative purposes and to give ourselves a potentially useful NMR handle, the congeneric yttrium complexes $[Y\{N(SiMe_3)_2\}_3]$ (**4**), $[Y\{N(SiMe_2H)_2\}_3\cdot(thf)_2]$ (**5**) and $[Y\{OSi(SiMe_3)_3\}_3\cdot(thf)_2]$ (**6**) were also prepared following similar synthetic protocols and isolated as crystalline materials in 58, 53 and 48% yield, respectively. The synthetic details and characterization for compounds **1-6** (Figure 1) and **7** are available in the Supporting Information (Figures S1–S21); note that the yields reported herein are for crystalline materials, and are therefore not optimized. Compound **1** (and **4**), where the Yb^{III} ion rests in an all-nitrogen environment, is the direct equivalent of the erbium complex $[Er\{N(SiMe_3)_2\}_3]$, reported in 2014 to be the first equatorially coordinated mononuclear Er-based SMM.[22] By contrast, in

Research Article
doi.org/10.1002/ceur.202400062

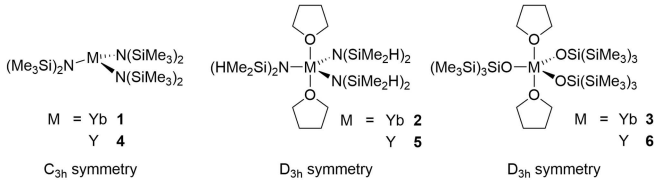

Figure 1. Schematic representation of compounds **1**–**6**.

complex **3**, the metal is surrounded by five oxygen-based ligands. Complex **2** features a N_3O_2 combination of nitrogen-based monoanionic amides and oxygen-based Lewis bases.

The molecular solid-state structures of complexes **1**–**3**, **6**, and **7** were established by single-crystal X-ray diffraction crystallography (see Figures 2, 3, and figures S15-S17 for the structures of **3**, **6**, and **7**). Although the structures of the Yb^{III} complexes **1** and **2** have already been reported,[23b,25–26] they are introduced here in the context of SMM studies along with a discussion of pertinent metric parameters and structural features. The structure of complex **1** was solved in the trigonal *P*-3 space group. It adopts a slightly pyramidalized trigonal planar arrangement, where the Yb^{III} ion sits 0.556(1) Å above the plane delineated by the three nitrogen atoms resulting in C_{3v} symmetry (Figure 2).

The interatomic Yb1–N1 distances of 2.180(7) Å is typically within the range for Yb^{III}-amides. The presence of Yb···H–C agostic interactions is indicated by the short Yb1–C5 interatomic distances, 2.888(8) Å. It is confirmed by the relatively acute Yb1–N1–Si1 angle of 106.6(3)°, much narrower than the other Yb1–N1–Si2 angle of 129.5(4)°, and by the near-perfect coplanarity of the Yb1, N1, Si1, and C5 atoms that feature a very small Yb1–N1–Si1–C5 torsion angle of 3.9(5)°. Accordingly, the Si2–C5 interatomic distance to the carbon atom involved in the agostic interaction (1.887(8) Å) is a little stretched compared to the other two Si2–C bonds (both 1.864(10) Å). These three agostic contacts are likely to induce the observed pyramidalization of the complex.[27] Note that data set for **1** was recorded herein at a lower temperature (150 K) than in the seminal report (298 K),[23b] which overall results in a marginally improved refinement (final $R_1 = 5.35$ vs 5.72%) and, more noticeably, a contracted volume ($V = 1906.1(2)$ vs 1980(1) Å^3).

Complex **2** crystallizes as a distorted trigonal bipyramid (tbp, $\tau_{5,av} = 0.65$)[28] where the three nitrogen atoms occupy the equatorial positions and the oxygens take the apical sites (Figure 3). The metal ion sits in the plane delineated by the three nitrogen atoms ($\Sigma_{0,N\text{-}Yb\text{-}N} = 359.98(7)°$), although the N2–Yb1–N3 angle (141.42(7)°) is much wider than the other two (108.77(7)° and 109.79(7)°). The similarity and the relatively large values of all Yb1–N_i–Si_j angles, in the range 111.00(9)°-121.18(9)°, militates against the presence of significant Yb···H–Si agostic interactions.[29]

The complex overall displays pseudo D_{3h} symmetry, although the O1–Yb1–O2 angle of 158.82(5)° deviates substantially from the ideal linearity expected for *tbp* geometry. The reason for this distortion is unclear, albeit simple packing effects cannot be ruled out.

Molecular geometries for **1** and **2** were confirmed by Continuous Shape Measurements (CShM)[30] (Table S1) on the calculated structure (*vide infra*). The solvated compound **2** shows symmetric trigonal bipyramidal coordination environment (D_{3h} site symmetry) with remarkably low CShM values. For **1**, the coordination is best described as a pyramidal geometry (C_{3v} site symmetry) because of the agostic interactions that tilt the Yb^{III} ion out of the mean plane delineated by the three nitrogen atoms (see Figure 2).

Theoretical Approach

In order to confirm that the target molecules possess the expected energetic scheme, CASSCF/RASSI-SO calculations were performed on both complexes **1** and **2** (See SI for computational details). Calculations were also carried out on **3**

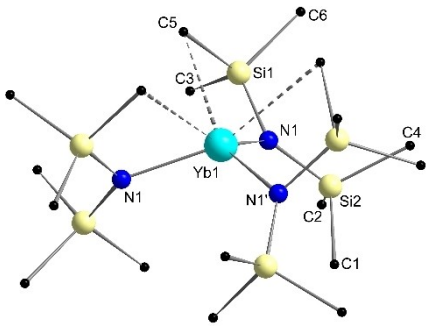

Figure 2. Representation of the molecular solid-state structure of [Yb{N(SiMe$_3$)$_2$}$_3$] (**1**). H atoms are omitted for clarity. Selected bond lengths (Å) and angles (°): Yb1–C5 = 2.888(8), Yb1–N1 = 2.180(7), Si2–C4 = 1.864(10), Si2–C5 = 1.887(8), Si2–C6 = 1.864(10); N1–Yb1–N1′ = 113.51(14), Yb1–N1–Si2 = 129.5(4), Yb1–N1–Si1 = 106.6(3). Symmetry operations used to generate equivalent N′ and N″ atoms: [1-y, x-y + 1, + z] and [y-x, 1-x, + z], respectively.

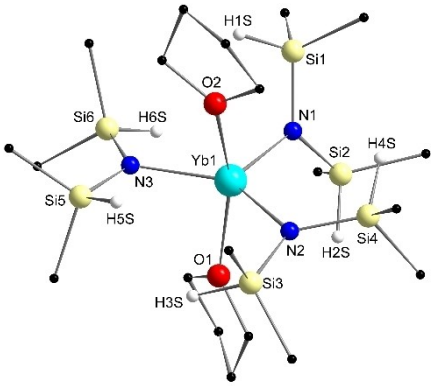

Figure 3. Representation of the molecular solid-state structure of [Yb{N(SiMe$_2$H)$_2$}$_3$·(thf)$_2$] (**2**). Except for those on silicon, atoms H atoms are omitted for clarity. Selected bond lengths (Å) and angles (°): Yb1–N1 = 2.1838(17), Yb1–N2 = 2.2349(17), Yb1–N3 = 2.2328(18), Yb1–O1 = 2.3532(13), Yb1–O2 = 2.3570(14), N1–Si1 = 1.7045(17), N1–Si2 = 1.7051(19), N2–Si3 = 1.7029(18), N2–Si4 = 1.7040(19), N3–Si5 = 1.695(2), N3–Si6 = 1.7071(19); N1–Yb1–N2 = 108.77(7), N1–Yb1–N3 = 109.79(7), N2–Yb1–N3 = 141.42(7), N1–Yb1–O1 = 99.61(6), N1–Yb1–O2 = 101.49(6), N2–Yb1–O1 = 88.65(5), N2–Yb1–O2 = 86.40(6), N3–Yb1–O1 = 83.83(5), N3–Yb1–O2 = 87.26(6), O1–Yb1–O2 = 158.82(5).

Research Article
doi.org/10.1002/ceur.202400062

for comparative purposes (Table S2 and Figures S22–S23). All atomic positions extracted from crystallographic outputs were optimized. Although this allowed us to obtain reliable molecular conformation for compound **2** bearing apical disordered thf molecules, the treatment was found unrealistic for **1**, since it induces a pronounced displacement of the Yb^{III} ion toward the center of the N3 plane defined by the three nitrogen ligands. Including dispersion corrections did not change the picture. Accordingly, for **1**, only the positions of the hydrogen atoms were optimized.

Pseudospin Hamiltonian tensors and wavefunction composition for the various multiplets obtained for compounds **1** and **2** are gathered in Table S2. On all derivatives, the ground state (KD1) shows high g_z values, very close to g_Z max = 8 μ_B, together with an almost pure $M_J = |7/2>$.

On the trigonal bipyramidal compound, **2**, a total energy splitting of 681 cm^{-1} is found together with a KD1-KD2 separation of 360 cm^{-1}. The wavefunction composition shows a very strong transverse component on KD2, that almost fully loses its magnetic anisotropy (Figure 4) and induces strong QTM as expected.[10] On the contrary, the tris-coordinated trigonal compound **1** shows remarkably pure wavefunction compositions of the excited states $M_J = |5/2>$, $|3/2>$, and $|1/2>$ for KD2 to KD4 (Figure 4 and Table S2) with a spectacular KD1-KD2 separation of 691 cm^{-1} and very high total energy splitting of 1312 cm^{-1}. The energy splitting is a little lower than predicted[11b] because of the slightly out-of-plane position of the Yb^{III}. When agostic interactions are canceled by full optimization of the atomic positions, the Yb^{III} lies back in the N3 plane and KD1-KD2 rises to 958 cm^{-1} providing an overall splitting of 1729 cm^{-1}; yet, as stated above, this treatment is not representative of the real geometry of the molecule. This is also reminiscent of the previous theoretical study on trigonal-planar Dy^{III} (oblate) and Er^{III} (prolate) derivatives where a similar influence of out-of-plane shift of the lanthanide has been observed.[31]

The magnetic anisotropies of **1** and **2** are depicted in Figure 5. They both show a very axial anisotropy of KD1, oriented perpendicular to the N3 plane. However, on **2** this axiality is lost on KD2. On the contrary **1** shows almost perfect axial anisotropy for KD1, KD2 and KD3 with $g_Z \gg g_X \approx g_Y \approx 0$ μ_B, while the opposite is seen on the highest KD4 with $M_J = |1/2>$ ($g_Z \approx 1 \ll g_X \approx g_Y$). This makes **1** a textbook example of a prolate SMM with almost ideal M_J splitting, magnetic tensor orientation and magnetic relaxation pathways, as very little QTM is evidenced on each KD.

Luminescence Investigations

In order to experimentally confirm the energy scheme obtained by *ab initio* calculation, we investigated the emission spectra of all compounds (see Figures S24–S34). Such a correlation between theoretical outcomes and luminescent properties is a convenient way to experimentally access lanthanide energetic schemes. This is particularly easy on Yb^{III}-SMM, which shows a line-shaped emission in the near-infrared (NIR) region made of four bands corresponding to the $^2F_{5/2} \rightarrow {}^2F_{7/2}$ transition that split

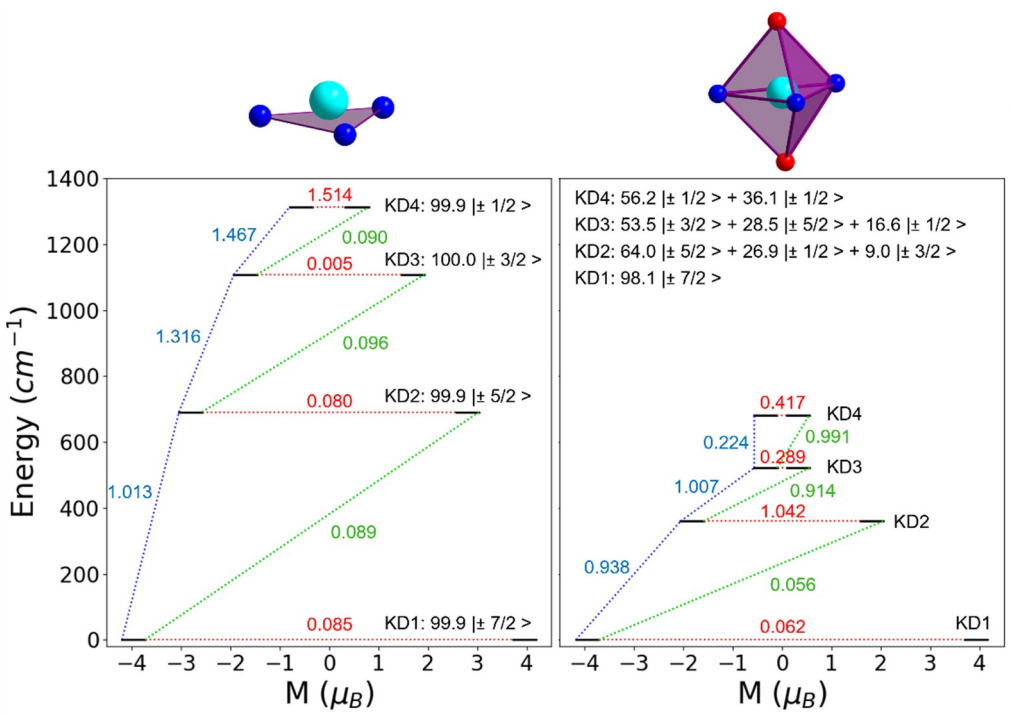

Figure 4. Energies (in cm^{-1}), wavefunction composition and projected μ_z (in μ_B) values along the ground magnetic axis for the 4 lowest Kramers doublets of **1** (left) and **2** (right). The values of the magnetic (*i.e.*, isotropic Zeeman) transition moments between the states are given for comparison. The values in red correspond to quantum tunnelling of the magnetization (for the ground state) and thermally-assisted quantum tunnelling of the magnetization (for the excited states) mechanisms of the magnetization relaxation, whereas blue and green values correspond to Orbach mechanisms.

Research Article
doi.org/10.1002/ceur.202400062

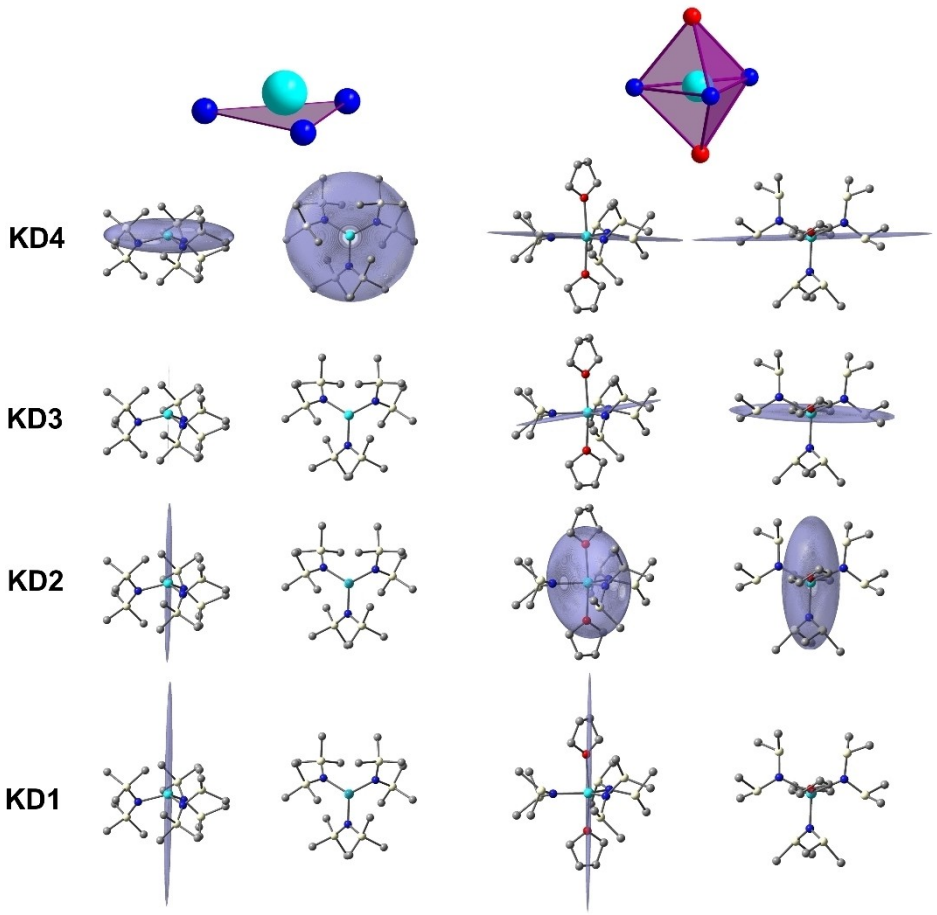

Figure 5. Representation of the calculated magnetic anisotropy tensors for the four lowest Kramers doublets of **1** (left) and **2** (right). Ellipsoids were generated as cube files using home-made aniso_to_cube tool[32] (the shape of the KD3 magnetic anisotropy tensor for 1 is so thin that it is almost a line with the same direction as KD1 and KD2).

into four sub-levels with $M_J = 7/2$, 5/2, 3/2 and 1/2.[33] The solid-state NIR emission spectra of **1** and **2** (Figure 6) differ substantially from what is usually observed with common Yb^{III} molecules.[34] The low symmetry of the Yb^{III} and its very high energy splitting induces a very large spanning of the characteristic four peaks. As a matter of example, in the spectrum of **1**

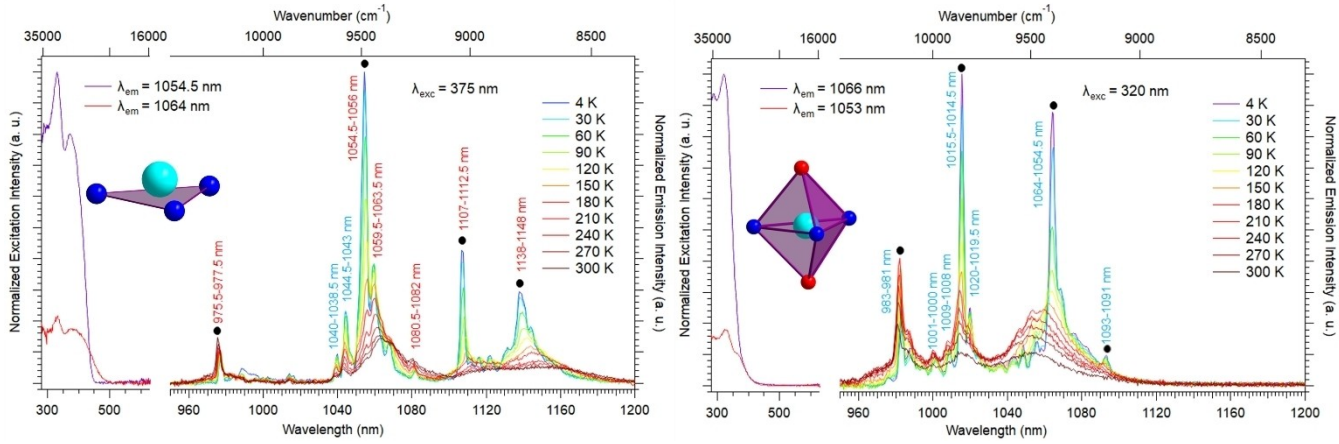

Figure 6. Solid-state excitation spectra at 4 K (purple spectrum) and 300 K (red spectrum) recorded at $\lambda_{em} = 1054.5$ nm or 1064 nm, respectively, and emission spectra ($\lambda_{exc} = 375$ nm) measured between 4 and 300 K of **1** (left). Solid-state excitation spectra at 4 K (purple spectrum) and 300 K (red spectrum) recorded at $\lambda_{em} = 1066$ nm or 1053 nm, respectively, and emission spectra ($\lambda_{exc} = 320$ nm) measured between 4 K and 300 K of **2** (right). Black dots indicate the peaks used for the determination of the KD splitting.

Research Article
doi.org/10.1002/ceur.202400062

recorded at 4 K, peaks are observed at 975.5 nm ($M_J = 7/2$), 1054.5 nm ($M_J = 5/2$), 1107 nm ($M_J = 3/2$) and 1138 nm ($M_J = 1/2$), corresponding to an M_J energy splitting of *ca.* 1500 cm^{-1}. More intriguing is the relative ratio between these four peaks, with the first one at 975.5 nm unusually small compared to the second, major one at 1054.5 nm. Additionally, this latter peak shows a unique structuration with five sub-speaks lying in the envelope of what would be the main peak if registered with a lower resolution; we are not aware of any other such example for molecular compounds. These last two prominent features are exacerbated for complex **1**, but have been observed on all compounds, including the Y-doped derivative $[Yb_{0.12}Y_{0.88}\{N(SiMe_3)_2\}_3]$ (aka **1'**, a mixture of **1** and **4** with Yb:Y = 12:88 mol-%; see Figures S18-S21), thus effectively ruling out a simple quenching effect between the emissive centers. As the temperature is raised, some of the peaks slightly shift and their structuration is lost. This phenomenon is under investigation, and will be the topic of a dedicated forthcoming publication.

The position of the peaks can be compared with the theoretical energy splitting considering the peak at lower energy as the zero-line (Figure 7 and Table S3). For all compounds, a good match is observed between the experimental and the theoretical calculations of the KD1-KD2 separation. This value can be compared with parameters extracted from the magnetic slow relaxation analysis (see hereafter).

Magnetic Investigation

Static magnetic measurements of compounds **1**-**3** (Figures S35–S71, and Tables S4–S16) show $\chi_M T_{(200K)}$ values close to the ones expected at room temperature for an isolated Yb^{III} ion, 2.57 emu.K.mol^{-1} ($J = 7/2$, $g = 8/7$). As expected, as the temperature is lowered, $\chi_M T$ shows a monotonous decrease as the M_J levels are depopulated, in line with theoretical predictions (Figures S35–S38). No significant magnetic hysteresis were observed down to 1.8 K (Figures S39–S46), except on **1'** where a very slight opening is visible. From the dynamic point-of-view, a slow magnetic relaxation was observed for all compounds only upon application of an optimal dc field estimated at 1700 Oe for **1** and **2** and 1900 Oe for **1'** (Figures S47–S49).

However, in line with theoretical findings, the magnetic behavior of **1** and **2** are strikingly different (Figures S50–S57). With **2**, a very common dynamic magnetic behavior is observed with the temperature dependence of the magnetic relaxation observed on a narrow temperature range (1.8–4 K), but with the advantage that Argand plots evidence a small distribution (α) of the relaxation rates and a very high relaxing fraction $(1-\chi_M')/\chi_T$ of almost 100% (Figure 8). Regarding **1**, very low α values and high relaxing fraction are also observed but with slow magnetic relaxation observed up to 9 K, one of the highest values reported for any Yb^{III}-SMM.

In order to investigate the influence of neighboring molecules on the magnetic behavior of **1**, its yttrium diluted $[Yb_{0.12}Y_{0.88}\{N(SiMe_3)_2\}_3]$ adduct (**1'**) has been measured too. The magnetic measurement for **1'** shows a temperature dependence of its magnetic relaxation similar to that seen for its non-diluted parent **1** (Figures S58–S63).

Temperature dependence of the relaxation rates (τ) of all compounds has been tentatively fitted by eq. 1. As frequently seen on compounds that do not show clear Orbach or QTM regimes, this approach is tedious and seems senseless. Indeed, different sets of equally robust solutions were obtained considering various combinations of relaxation pathways (Figure 9). This includes Orbach-like relaxation with small U_{eff} values in line with those of previously reported Yb^{III}-SMM. However, in our case, we benefit from the very high energy splitting calculated (Table S2) and observed (Figure 6) to rule out such solutions. By Arrhenius fit of $\ln(\tau)$ vs 1/T, the following values were obtained: $C = 0.20 \pm 0.03\ s^{-1}K^{-n}$, $n = 5.12 \pm 0.08$, $\tau_{QTM} = 0.03 \pm 0.01$ s (**1**), $C = 0.03 \pm 0.01\ s^{-1}K^{-n}$, $n = 6.04 \pm 0.05$, $\tau_{QTM} = 0.26 \pm 0.01$ s (**1'**), $C = 0.06 \pm 0.01\ s^{-1}K^{-n}$, $n = 9.23 \pm 0.07$, $\tau_{QTM} = 0.02 \pm 0.01$ s (**2**) (see Table S13). For all compounds, Raman-like and QTM relaxation operate, the latter being reduced for **1'** in comparison with **1** because of magnetic dilution. Considering

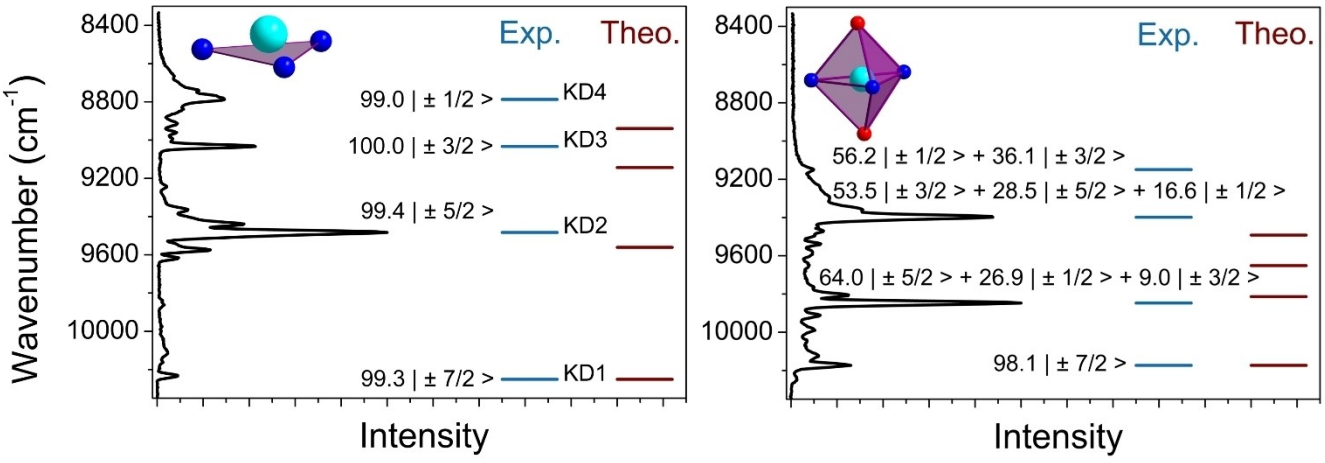

Figure 7. Solid-state emission spectra ($\lambda_{exc} = 375$ nm) measured at 4 K for **1** (left) and **2** (right) and comparison with the ground state splitting extracted from calculations from lowest (KD1) to highest (KD4).

Research Article
doi.org/10.1002/ceur.202400062

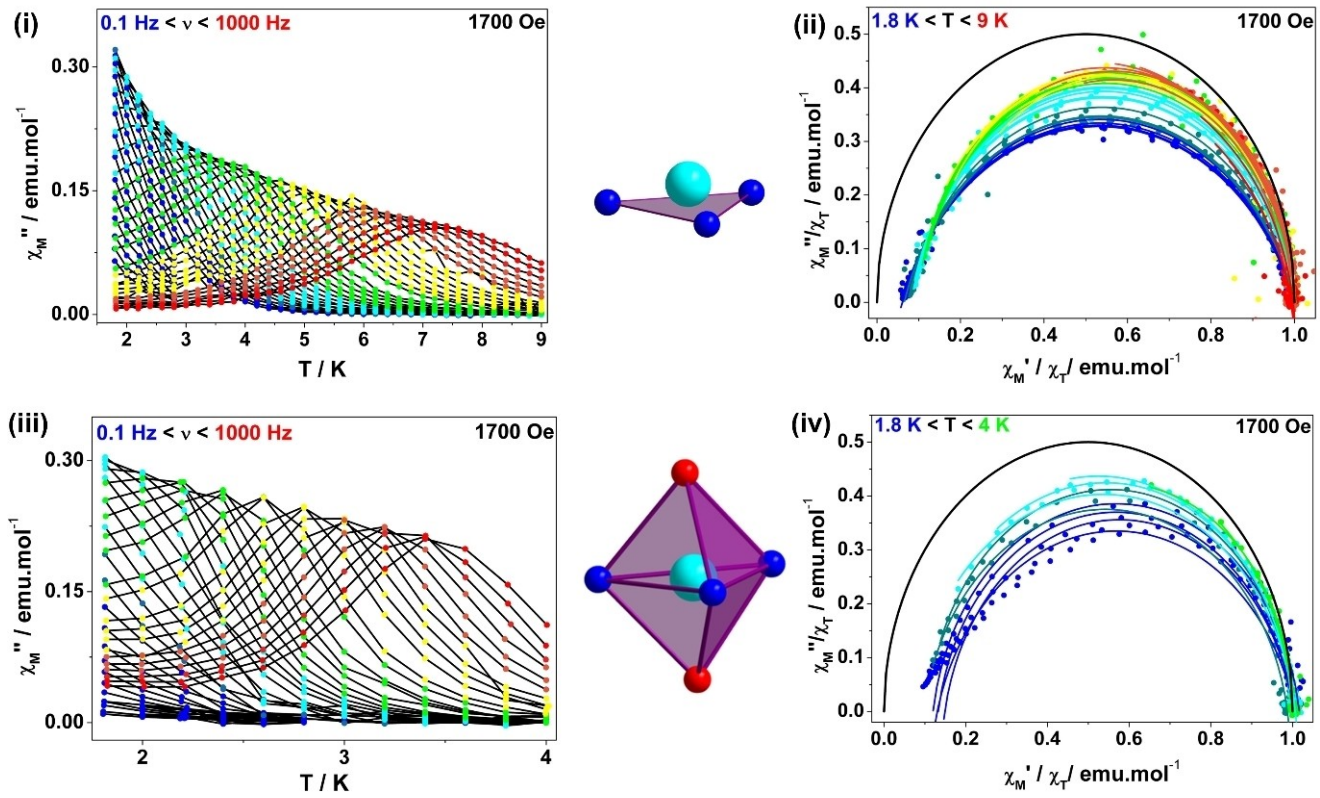

Figure 8. Dynamic magnetic measurements performed on solid samples of **1** (top line) and **2** (bottom line) under $H_{dc} = 1700$ Oe. (Left column) Temperature dependence of out-of-phase susceptibility χ_M'' measured from 0.1 Hz (blue) to 1000 Hz (red). (Right column) Argand plot normalized over the isothermal susceptibility (χ_T) with coloured lines that represent the best fits as calculated with an extended Debye model. The black line is the simulated Argand plot for an ideal single relaxation process with no distribution of the relaxation times ($\alpha = 0$) and an adiabatic susceptibility, χ_s, equal to 0.

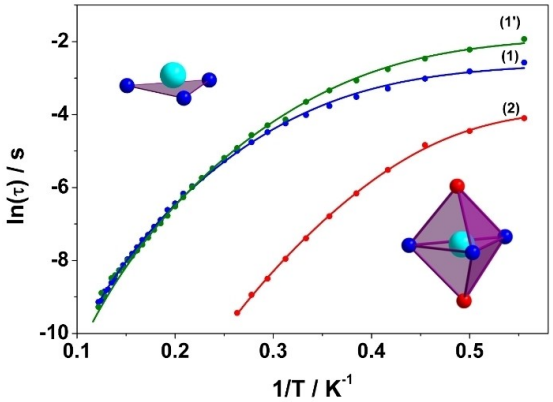

Figure 9. Temperature dependence of the relaxation times of **1**, **1′**, and **2** obtained with optimal H_{dc} field of 1700 Oe (**1** and **2**) and 1900 Oe (**1′**) and best fits considering Raman and QTM relaxation as lines (see text).

direct relaxation does not provide any improvement. (Figures S72–S75)

Consequently, one is led to wonder whether the values of U_{eff} reported to date in the literature for Yb^{III}-SMM that match small theoretical KD1-KD2 splittings are not simple artefacts, and it is plausible that Orbach relaxation actually did not operate with most of the reported Yb^{III}-SMM.

Discussion

Theoretical and luminescent investigations clearly demonstrate that compounds **1** and **2** possess the predicted high M_J splitting.[10] In particular, the almost ideal trigonal planar environment of **1** provides an astonishingly large separation of the Yb^{III} emission peaks. Similarly, the predicted effect of the switch from trigonal planar to trigonal bipyramidal by capping neutral molecules is actually observed, and it induces the expected halving of the total splitting from **1** to **2**.

However, the resulting magnetic behavior does not benefit from this strong splitting, and SMM relaxation is seen at modest temperatures on the close-to-perfect trigonal planar derivatives **1** and **1′**. In other words, despite their optimal geometry and charge localization, the reported compounds are mild SMMs showing mainly Raman-like relaxation, and they do not exhibit significant magnetic hysteresis. This is reminiscent of similar findings on low-coordinate Dy^{III}-SMM that were theorized to have extremely large energy splitting, but behaved well below expectations[9a] and where the influence of spin-phonon coupling was suspected.

For most Yb^{III}-SMMs, the absence of slow relaxation in zero field is simply attributed to the large transverse component of the ground or first excited KDs, as recently observed for example on chiral Yb^{III}-SMM,[35] bis-coordinated Yb^{III}-SMM[13] or double-bridged Yb^{III}_2-SMM[36] that depict magnetic relaxation up

Research Article
doi.org/10.1002/ceur.202400062

to temperatures similar as those observed for **1**. However, in **1**, the almost pure composition of the wavefunction of the various KDs rules out this hypothesis as a cause for mild SMM behavior.

It is very likely that the discrepancy between *ab initio* calculations and magnetic observation is linked to the way the molecules exchange energy with their surroundings.[37] Indeed, phonon-driven magnetic relaxation (Orbach and Raman) is affected by vibrational modes of the surrounding molecules, either via spin-lattice relaxation[38] or vibronic coupling.[39] This is particularly true on **1**, which is expected to depict a large variety of vibration modes because the ligands are small and not rigid. Recent studies on Kramers SMM have shown that spin-phonon coupling can be operative and influence QTM even when no vibrational excitation can be expected.[40] Indeed, vibronic coupling[41] has been recently calculated[42] and measured by FIRMS[43] on the [Yb(trensal)] SMM[6] and [Er{N-(SiMe$_3$)$_2$}$_3$],[22] showing that motion modes in the first coordination sphere are those that are the most coupled with the electronic states. Finally, it is worth noting that the O5 trigonal bipyramidal derivative, **3**, features decent SMM behavior (Figures S64–S71), suggesting that a trigonal planar O3 coordination environment, if accessible, could lead to enhanced Yb^{III}-SMM properties.

Conclusions

The present work is the first experimental investigation of optimal SMM based on lanthanide prolate ions, by applying a combined synthetic, magnetic, optical and theoretical approach. Our findings corraborate the theoretical prediction made on purely theroretical objects,[10] but also highlight that further molecular engineering is required to reach high magnetic perfomance with such molecules.

Indeed, many Yb^{III}-SMMs have been reported to date, few improvements in their magnetic behavior have been observed, in contrast with Dy^{III}-SMMs. This is mainly due to the difficulty in controlling the first coordination sphere in Yb^{III} complexes, as exclusively equatorial coordination for low-coordinate lanthanides is not easily accessible. Such a geometry has been predicted on hypothetical compounds to induce the greatest possible splitting for Yb^{III}, with little QTM pollution.[10] To test the theoretical predictions, we have synthesized an almost planar trigonal compound **1** that matches the predicted ideal trivalent geometry, and its bipyramidal trigonal congener **2**. The seminal theoretical calculations are hence now confirmed by these real molecules, which also corroborate the severe influence of capping ligands on the splitting and purity of the composition of the wavefunction of the Kramers doublets.

Low-temperature NIR emission experimentally confirms the $^2F_{7/2}$ ground state splitting and shows remarkably sophisticated and extended emission spectra. Magneto-luminescent correlations have been established, showing that Orbach relaxation is unlikely to drive the behavior of these Yb^{III}-SMMs. This is also probably true of the previously reported Yb^{III}-SMM, whose small Kramers doublets splitting fortuitously match the high-temperature trend of Raman-like relaxation.

In spite of optimal molecular engineering, the magnetic behavior of Yb^{III}-SMM does not improve as much as predictions suggested, even if relaxation is observed up to 9 K. This could be due to the high flexibility of the coordinating ligands, inducing strong vibronic coupling that proved detrimental to the magnetic relaxation as shown before on Dy^{III}-SMMs; as illustrated herein, Yb^{III}-SMM makes no exception. We are currently exploring this line of investigation. Future works should focus on the design of rigid, and probably polydentate, equatorial ligands in order to stabilize trigonal planar geometries and provide Yb^{III}-SMM able to operate in the absence of an external field.

Supporting Information

The authors have cited additional references within the Supporting Information[44–67] that contains all additional data supporting this article including structural, theoretical, magnetic and luminescence investigations. Deposition Number(s) https://www.ccdc.cam.uk/services?id=doi:anie.202408133, 2348421 (for **1**), 2348422 (for **2**),2348423 (for **3**), 2348424 (for **6**), 2348425 (for **7**) contain the supplementary crystallographic data for this paper. These data are provided free of charge by the joint Cambridge Crystallographic Data Centre.

Acknowledgements

The authors acknowledge Région Bretagne for the provision of SAD 2022 research grant (MOL4DATA), CPER Mat&Trans for low-temperature optical cryostat funding, Rennes Metropole, and INSA Rennes. B.L.G. thanks the French GENCI/IDRIS-CINES centers for high-performance computing resources. Thierry Guizouarn from ISCR "Centre de mesures physiques" is thanked for his assistance in collecting magnetic data. Stephane Freslon and Laura Le Breton from INSA Rennes are acknowledged for their help in EDS/SEM analyses. We are grateful to O. Maury and A. Lunghi for stimulating discussions.

Conflict of Interests

The authors declare no conflict of interest.

Data Availability Statement

The data that support the findings of this study are available from the corresponding author upon reasonable request.

Keywords: lanthanides · luminescence · prolate · single-molecule magnets · ytterbium(III)

[1] K. Bernot, *Eur. J. Inorg. Chem.* **2023**, *26*, e202300336.
[2] J. D. Rinehart, J. R. Long, *Chem. Sci.* **2011**, *2*, 2078–2085.

Research Article
doi.org/10.1002/ceur.202400062

[3] a) F. Pointillart, O. Cador, B. Le Guennic, L. Ouahab, *Coord. Chem. Rev.* **2017**, *346*, 150–175; b) A. Borah, R. Murugavel, *Coord. Chem. Rev.* **2022**, *453*, 214288.
[4] J. Wang, C.-Y. Sun, Q. Zheng, D.-Q. Wang, Y.-T. Chen, J.-F. Ju, T.-M. Sun, Y. Cui, Y. Ding, Y.-F. Tang, *Chem. Asian J.* **2023**, *18*, e202201297.
[5] J. Moutet, J. Schleinitz, L. La Droitte, M. Tricoire, F. Pointillart, F. Gendron, T. Simler, C. Clavaguéra, B. Le Guennic, O. Cador, G. Nocton, *Angew. Chem. Int. Ed.* **2021**, *60*, 6042–6046.
[6] D. Errulat, K. L. M. Harriman, D. A. Gálico, E. V. Salerno, J. van Tol, A. Mansikkamäki, M. Rouzières, S. Hill, R. Clérac, M. Murugesu, *Nat. Commun.* **2024**, *15*, 3010.
[7] a) J. Li, Y. Yang, Q. Yu, G. Su, W. Liu, *J. Phys. Chem. C* **2024**, *12*, 4882–4890; b) V. Vieru, S. Gómez-Coca, E. Ruiz, L. F. Chibotaru, *Angew. Chem. Int. Ed.* **2024**, *63*, e202303146.
[8] a) F. Ortu, D. P. Mills, in *Handbook on the Physics and Chemistry of Rare Earths, Vol. 55* (Eds.: J.-C. G. Bünzli, V. K. Pecharsky), Elsevier, **2019**, pp. 1–87; b) A. K. Bar, P. Kalita, M. K. Singh, G. Rajaraman, V. Chandrasekhar, *Coord. Chem. Rev.* **2018**, *367*, 163–216.
[9] a) J. Emerson-King, G. K. Gransbury, G. F. S. Whitehead, I. J. Vitorica-Yrezabal, M. Rouzières, R. Clérac, N. F. Chilton, D. P. Mills, *J. Am. Chem. Soc.* **2024**, *146*, 3331–3342; b) A. H. Vincent, Y. L. Whyatt, N. F. Chilton, J. R. Long, *J. Am. Chem. Soc.* **2023**, *145*, 1572–1579.
[10] M. Amoza, S. Gómez-Coca, E. Ruiz, *Phys. Chem. Chem. Phys.* **2021**, *23*, 1976–1983.
[11] a) C. A. P. Goodwin, F. Ortu, D. Reta, N. F. Chilton, D. P. Mills, *Nature* **2017**, *548*, 439–442; b) F.-S. Guo, B. M. Day, Y.-C. Chen, M.-L. Tong, A. Mansikkamäki, R. A. Layfield, *Science* **2018**, *362*, 1400–1403.
[12] N. F. Chilton, C. A. P. Goodwin, D. P. Mills, R. E. P. Winpenny, *Chem. Commun.* **2015**, *51*, 101–103.
[13] D. Errulat, K. L. M. Harriman, D. A. Gálico, A. A. Kitos, A. Mansikkamäki, M. Murugesu, *Nat. Chem.* **2023**, *15*, 1100–1107.
[14] M. E. Boulon, G. Cucinotta, J. Luzon, C. Degl'Innocenti, M. Perfetti, K. Bernot, G. Calvez, A. Caneschi, R. Sessoli, *Angew. Chem. Int. Ed.* **2013**, *52*, 350–354.
[15] M. Perfetti, F. Pointillart, O. Cador, L. Sorace, L. Ouahab, in *Molecular Magnetic Materials*, Wiley-VCH Verlag GmbH & Co. KGaA, **2017**, pp. 345–368.
[16] G. Cucinotta, M. Perfetti, J. Luzon, M. Etienne, P.-E. Car, A. Caneschi, G. Calvez, K. Bernot, R. Sessoli, *Angew. Chem. Int. Ed.* **2012**, *51*, 1606–1610.
[17] S. T. Liddle, J. van Slageren, *Chem. Soc. Rev.* **2015**, *44*, 6655–6669.
[18] a) J. Long, Y. Guari, R. A. S. Ferreira, L. D. Carlos, J. Larionova, *Coord. Chem. Rev.* **2018**, *363*, 57–70; b) R. Marin, G. Brunet, M. Murugesu, *Angew. Chem. Int. Ed.* **2021**, *60*, 1728–2746; c) J. Larionova, Y. Guari, S. Sene, G. Félix, in *Handbook on the Physics and Chemistry of Rare Earths, Vol. 64* (Eds.: J.-C. G. Bunzli, S. M. Kauzlarich), Elsevier, **2023**, pp. 93–173.
[19] K. S. Pedersen, J. Dreiser, H. Weihe, R. Sibille, H. V. Johannesen, M. A. Sørensen, B. E. Nielsen, M. Sigrist, H. Mutka, S. Rols, J. Bendix, S. Piligkos, *Inorg. Chem.* **2015**, *54*, 7600–7606.
[20] S. Gómez-Coca, D. Aravena, R. Morales, E. Ruiz, *Coord. Chem. Rev.* **2015**, *289–290*, 379–392.
[21] G. Rajaraman, S. K. Singh, T. Gupta, M. Shanmugam, *Chem. Commun.* **2014**, *50*, 15513–15516.
[22] P. Zhang, L. Zhang, C. Wang, S. Xue, S.-Y. Lin, J. Tang, *J. Am. Chem. Soc.* **2014**, *136*, 4484–4487.
[23] a) D. C. Bradley, J. S. Ghotra, F. A. Hart, *J. Chem. Soc. Dalton Trans.* **1973**, 1021–1023; b) M. Niemeyer, *Z. Anorg. Allg. Chem.* **2002**, *628*, 647–657; c) P. G. Eller, D. C. Bradley, M. B. Hursthouse, D. W. Meek, *Coord. Chem. Rev.* **1977**, *24*, 1–95; d) J. S. Ghotra, M. B. Hursthouse, A. J. Welch, *J. Chem. Soc. Chem. Commun.* **1973**, 669–670.
[24] W. A. Herrmann, R. Anwander, F. C. Munck, W. Scherer, V. Dufaud, N. W. Huber, G. R. J. Artus, *Z. Naturforsch. B* **1994**, *49*, 1789–1797.
[25] T. J. Boyle, F. Guerrero, R. E. Cramer, P. C. Reuel, D. M. Boye, H. L. Brooks, *Inorg. Chem.* **2022**, *61*, 5048–5059.
[26] G. Occhipinti, C. Meermann, H. M. Dietrich, R. Litlabø, F. Auras, K. W. Törnroos, C. Maichle-Mössmer, V. R. Jensen, R. Anwander, *J. Am. Chem. Soc.* **2011**, *133*, 6323–6337.
[27] M. P. Conley, G. Lapadula, K. Sanders, D. Gajan, A. Lesage, I. del Rosal, L. Maron, W. W. Lukens, C. Copéret, R. A. Andersen, *J. Am. Chem. Soc.* **2016**, *138*, 3831–3843.
[28] A. W. Addison, T. N. Rao, J. Reedijk, J. Vanrijn, G. C. Verschoor, *J. Chem. Soc. Dalton Trans.* **1984**, 1349–1356.
[29] W. Hieringer, J. Eppinger, R. Anwander, W. A. Herrmann, *J. Am. Chem. Soc.* **2000**, *122*, 11983–11994.
[30] S. Alvarez, P. Alemany, D. Casanova, J. Cirera, M. Llunell, D. Avnir, *Coord. Chem. Rev.* **2005**, *249*, 1693–1708.
[31] T. Gupta, G. Rajaraman, *Eur. J. Inorg. Chem.* **2018**, *2018*, 3402–3412.
[32] R. Marchal, B. Le Guennic, K. Bernot, https://gitlab.com/remimarchal56/aniso_to_cube**2024**.
[33] a) W.-B. Chen, L. Zhong, Y.-J. Zhong, Y.-Q. Zhang, S. Gao, W. Dong, *Inorg. Chem. Front.* **2020**, *7*, 3136–3145; b) K. Soussi, J. Jung, F. Pointillart, B. Le Guennic, B. Lefeuvre, S. Golhen, O. Cador, Y. Guyot, O. Maury, L. Ouahab, *Inorg. Chem. Front.* **2015**, *2*, 1105–1117; c) Q.-W. Li, J.-L. Liu, J.-H. Jia, Y.-C. Chen, J. Liu, L.-F. Wang, M.-L. Tong, *Chem. Commun.* **2015**, *51*, 10291–10294; d) J. Ruiz, G. Lorusso, M. Evangelisti, E. K. Brechin, S. J. A. Pope, E. Colacio, *Inorg. Chem.* **2014**, *53*, 3586–3594.
[34] F. Guégan, J. Jung, B. Le Guennic, F. Riobé, O. Maury, B. Gillon, J.-F. Jacquot, Y. Guyot, C. Morell, D. Luneau, *Inorg. Chem. Front.* **2019**, *6*, 3152–3157.
[35] K. Dhbaibi, M. Grasser, H. Douib, V. Dorcet, O. Cador, N. Vanthuyne, F. Riobé, O. Maury, S. Guy, A. Bensalah-Ledoux, B. Baguenard, G. L. J. A. Rikken, C. Train, B. Le Guennic, F. Pointillart, M. Atzori, J. Crassous, *Angew. Chem. Int. Ed.* **2023**, *62*, e202215558.
[36] S. Konar, A. Mondal, *Chem. Eur. J.* **2021**, *27*, 3449–3456.
[37] A. Lunghi, S. Sanvito, *Nat. Chem. Rev.* **2022**, *6*, 761–781.
[38] S. Mondal, A. Lunghi, *J. Am. Chem. Soc.* **2022**, *144*, 22965–22975.
[39] A. L. Blockmon, A. Ullah, K. D. Hughey, Y. Duan, K. R. O'Neal, M. Ozerov, J. J. Baldoví, J. Aragó, A. Gaita-Ariño, E. Coronado, J. L. Musfeldt, *Inorg. Chem.* **2021**.
[40] A. Mattioni, J. K. Staab, W. J. A. Blackmore, D. Reta, J. Iles-Smith, A. Nazir, N. F. Chilton, *Nat. Commun.* **2024**, *15*, 485.
[41] J. G. C. Kragskow, A. Mattioni, J. K. Staab, D. Reta, J. M. Skelton, N. F. Chilton, *Chem. Soc. Rev.* **2023**, *52*, 4567–4585.
[42] R. Nabi, J. K. Staab, A. Mattioni, J. G. C. Kragskow, D. Reta, J. M. Skelton, N. F. Chilton, *J. Am. Chem. Soc.* **2023**, *145*, 24558–24567.
[43] a) J. G. C. Kragskow, J. Marbey, C. D. Buch, J. Nehrkorn, M. Ozerov, S. Piligkos, S. Hill, N. F. Chilton, *Nat. Commun.* **2022**, *13*, 825; b) D. H. Moseley, S. E. Stavretis, Z. Zhu, M. Guo, C. M. Brown, M. Ozerov, Y. Cheng, L. L. Daemen, R. Richardson, G. Knight, K. Thirunavukkuarasu, A. J. Ramirez-Cuesta, J. Tang, Z.-L. Xue, *Inorg. Chem.* **2020**, *59*, 5218–5230.
[44] J. Eppinger, E. Herdtweck, R. Anwander, *Polyhedron* **1998**, *17*, 1195–1201.
[45] a) Schwarzenbach, G.; Flaschka, H. "Complexometric Titrations"; Methuen: London, 1969; p 19; b) W. J. Evans, S. C. Engerer, K. M. Coleson, *J. Am. Chem. Soc.* **1981**, *103*, 6672–6677.
[46] A. M. Bienfait, C. Schädle, C. Maichle-Mössmer, K. W. Törnroos, R. Anwander, *Dalton Trans.* **2014**, *43*, 17324–17332.
[47] T. J. Woodman, Y. Sarazin, G. Fink, K. Hauschild, M. Bochmann, *Macromolecules* **2005**, *38*, 3060–3067.
[48] G. M. Sheldrick, *Acta Crystallogr.* **2015**, *A71*, 3–8.
[49] G. M. Sheldrick, *Acta Crystallogr.* **2015**, *C71*, 3–8.
[50] P. v d Sluis, A. L. Spek, *Acta Crystallogr.* **1990**, *A46*, 194–201.
[51] A. L. Spek, *J. Appl. Crystallogr.* **2003**, *36*, 7–13.
[52] I. F. Galván, M. Vacher, A. Alavi, C. Angeli, F. Aquilante, J. Autschbach, J. J. Bao, S. I. Bokarev, N. A. Bogdanov, R. K. Carlson, L. F. Chibotaru, J. Creutzberg, N. Dattani, M. G. Delcey, S. S. Dong, A. Dreuw, L. Freitag, L. M. Frutos, L. Gagliardi, F. Gendron, A. Giussani, L. González, G. Grell, M. Guo, C. E. Hoyer, M. Johansson, S. Keller, S. Knecht, G. Kovačević, E. Källman, G. Li Manni, M. Lundberg, Y. Ma, S. Mai, J. P. Malhado, P. Å. Malmqvist, P. Marquetand, S. A. Mewes, J. Norell, M. Olivucci, M. Oppel, Q. M. Phung, K. Pierloot, F. Plasser, M. Reiher, A. M. Sand, I. Schapiro, P. Sharma, C. J. Stein, L. K. Sørensen, D. G. Truhlar, M. Ugandi, L. Ungur, A. Valentini, S. Vancoillie, V. Veryazov, O. Weser, T. A. Wesołowski, P.-O. Widmark, S. Wouters, A. Zech, J. P. Zobel, R. Lindh, *J. Chem. Theory Comput.* **2019**, *15*, 5925–5964.
[53] B. O. Roos, P. R. Taylor, P. E. M. Siegbahn, *Chem. Phys.* **1980**, *48*, 157–173.
[54] P.-A. Malmqvist, B. O. Roos, B. Schimmelpfennig, *Chem. Phys. Lett.* **2002**, *357*, 230–240.
[55] P.-A. Malmqvist, B. O. Roos, *Chem. Phys. Lett.* **1989**, *155*, 189–194.
[56] B. A. Heß, C. M. Marian, U. Wahlgren, O. Gropen, *Chem. Phys. Lett.* **1996**, *251*, 365–371.
[57] L. F. Chibotaru, L. Ungur, *J. Chem. Phys.* **2012**, *137*, 064112.
[58] L. F. Chibotaru, L. Ungur, A. Soncini, *Angew. Chem. Int. Ed.* **2008**, *47*, 4126–4129.
[59] F. Aquilante, P.-A. Malmqvist, T. B. Pedersen, A. Ghosh, B. O. Roos, *J. Chem. Theory Comput.* **2008**, *4*, 694–702.
[60] B. O. Roos, R. Lindh, P.-A. Malmqvist, V. Veryazov, P.-O. Widmark, *J. Phys. Chem. A* **2004**, *108*, 2851–2858.
[61] B. O. Roos, R. Lindh, P.-A. Malmqvist, V. Veryazov, P.-O. Widmark, A.-C. Borin, *J. Phys. Chem. A* **2008**, *112*, 11431–11435.

Research Article
doi.org/10.1002/ceur.202400062

[62] G. te Velde, F. M. Bickelhaupt, E. J. Baerends, C. Fonseca Guerra, S. J. A. van Gisbergen, J. G. Snijders, T. Ziegler, *J. Comb. Chem.* **2001**, *22*, 931–967.
[63] AMS 2022.103, Amsterdam, The Netherlands, http://www.scm.com.
[64] J. P. Perdew, K. Burke, M. Ernzerhof, *Phys. Rev. Lett.* **1996**, *77*, 3865–3868.
[65] J. P. Perdew, K. Burke, M. Ernzerhof, *Phys. Rev. Lett.* **1997**, *78*, 1396.
[66] E. van Lenthe, E. J. Baerends, *J. Comput. Chem.* **2003**, *24*, 1142–1156.
[67] D. Reta, N. F. Chilton, *Phys. Chem. Chem. Phys.* **2019**, *21*, 23567.
[68] W. J. A. Blackmore, G. K. Gransbury, P. Evans, J. G. C. Kragskow, D. P. Mills, N. F. Chilton, *Phys. Chem. Chem. Phys.* **2023**, *25*, 16735–16744.

Version of record online: ■■, ■■

RESEARCH ARTICLE

When ideal is not enough: investigation of the very large ground state splitting of planar tris-coordinated Yb^{III} ion and its consequence on luminescent and single-molecule magnet properties. We demonstrate that specifically designed textbook examples of prolate SMMs show the expected very large ground state splittings but that this latter is not enough to induce efficient SMM behavior.

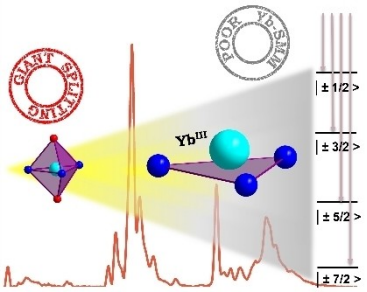

Dr. N. Jain, Dr. F. Houard, R. Marchal, M. Cordier, Dr. B. Le Guennic, Dr. Y. Suffren, Dr. Y. Sarazin, Prof. K. Bernot**